Journal of Power Sources 257 (2014) 388–393

Contents lists available at ScienceDirect

Journal of Power Sources

journal homepage: www.elsevier.com/locate/jpowsour

Development and characterization of Li-ion capacitor pouch cells

W.J. Cao [a,b], J. Shih [a,b], J.P. Zheng [a,b,c,*], T. Doung [d]

[a] Department of Electrical and Computer Engineering, Florida A&M University and Florida State University, Tallahassee, FL 32310, USA
[b] Aero-Propulsion, Mechatronics and Energy (AME) Center, Florida State University, Tallahassee, FL 32310, USA
[c] Center for Advanced Power Systems (CAPS), Florida State University, Tallahassee, FL 32310, USA
[d] Office of Vehicle Technologies, U.S. Department of Energy, Annandale, VA 22003, USA

HIGHLIGHTS

- The specific energy and energy density are 30 Wh kg^{-1} and 39 Wh L^{-1}, respectively.
- The capacitor was discharge at rates over 100 C rate.
- The capacitor was cycled over 10,000 cycles with capacitance degradation <20%.

ARTICLE INFO

Article history:
Received 25 November 2013
Received in revised form
7 January 2014
Accepted 17 January 2014
Available online 24 January 2014

Keywords:
Li-ion capacitor
Pouch cells
Activated carbon
Hard carbon
SLMP
Pore size distribution

ABSTRACT

High energy density Li-ion capacitor (LIC) pouch cell prototypes were assembled with lab-scale equipment using activated carbon cathode and hard carbon/lithium stabilized metal power (SLMP) anode. The specific energy and energy density as high as 30 Wh kg^{-1} and 39 Wh L^{-1} have been achieved, respectively. The pouch cells can deliver over 50% of the maximum stored energy at a discharge rate over 100 C-rate. After 10,000 cycles, the LIC pouch cell still has 80% of the initial capacitance. The average leakage current is 0.3 μA cm^{-2} during the first 72 h.

1. Introduction

Lithium-ion Capacitors (LICs) have attracted much attention as a new power source due to its high energy density compared to conventional electric double-layer capacitors (EDLCs), and its high power density compared to batteries as well as having the long cycle life. LICs contain a lithium-ion battery (LIB) anode electrode and an EDLC cathode electrode [1–3]. Extensive research has been done to optimize the electrochemical performance of the LICs [4–16]. Recently, Balducci et al. [17] reported the use of carbon coated iron oxide-based electrodes for the anode for LICs. Schroeder et al. [18] used soft carbon for the anode for LICs to achieve high power density and long cycle life. Smith et al. [19] have done research into the electrochemical performance and thermal behavior of LICs, and the maximum energy density of the LIC pouch cells was approximately 10–15 Wh kg^{-1}. The LIC cells used in Smith's group were obtained from JM Energy and contained a third electrode of Li metal to pre-dope the anode electrodes, which was first proposed by Fuji Co. [6].

Previously, we have reported a LIC with carbon cathode and hard carbon/SLMP anode electrodes with high energy density, high power density and long cycle life [20,21]. This was made possible by replacing the conventional activated carbon anode of EDLCs with hard carbon (HC) with stabilized lithium metal powder (SLMP) on its surface. The added SLMP increased the open circuit voltage of the LIC and ensured less salt to be consumed when the LIC was charged, which was the reason for the high energy density. The charge–discharge maximum voltage of the LIC could be achieved as

* Corresponding author. Center for Advanced Power Systems (CAPS), Florida State University, Tallahassee, FL 32310, USA.
E-mail address: zheng@eng.fsu.edu (J.P. Zheng).

0378-7753/$ – see front matter © 2014 Published by Elsevier B.V.
http://dx.doi.org/10.1016/j.jpowsour.2014.01.087

high as 4.1 V with stable cycling performance [22]. During our LIC cell assembly, a conventional two-electrode structure was used, and the SLMP was applied onto the surface of the hard carbon anode electrodes and some of Li from the SLMP was intercalated into the hard carbon when the electrolyte was filled into the cell. This high energy density concept of the LICs with such novel structure has already been demonstrated by laboratorial coin cells [22]. However, the LIC pouch cells with such novel electrode composition and the two-electrode structure have not been reported by any research group. Therefore, in this paper, we wish to report the detailed performance of two LIC pouch cells LIC250 and LIC395. The comparison of the energy and power performance between LIC250 and LIC395 is also included in this paper.

2. Experimental

Commercial active materials were used for both the positive and negative electrodes as received. The positive electrode (PE) was prepared by coating a slurry mixture of activated carbon (AC) and polytetrafluoroethylene (PTFE) as a binder by the mass ratio of 90:10 on an Al foil substrate (Exopack™, 20 μm in thickness). Two kinds of AC materials including YP-50F (Kuraray Chemical Co, Japan) and AB-520 (MTI Corporation; USA) were used to manufacture the cathode electrodes. The slurry mixture of the negative electrode (NE) was made of hard carbon (HC, Carbotron P(J), Kureha Japan) and PTFE as a binder by the mass ratio of 92:8. After the slurry was prepared, it was coated onto a Cu foil substrate that had a thickness of 10 μm. Then the electrodes were dried at 100 °C for 2 h in oven with flowing air. After all the electrodes were dried, a hot-roll pressing was applied to the AC and HC electrode sheets to make them into the desired thickness, 150 μm for AC and 90 μm for HC. All the electrode sheets were kept in the dry room and punched out into 8 × 5 cm (active area) electrodes with additional 1 cm long tab. All the electrodes were dried again at 120 °C for overnight in a vacuum oven then the stabilized lithium metal powder (SLMP) was applied onto the surface of all the prefabricated HC anode electrodes by doctor blade method and then roll-pressing in a dry room as shown in Fig. 1 before being assembled into the pouch cell. The SLMP, which is purchased from FMC Lithium, is Li powder with a passivation layer at surface and the average size of the Li powder is ~40 μm. Fig. 2(a) displays the 8 × 5 cm anode electrode with additional 1 cm long Cu tab before loading the SLMP. After all the SLMP was pressed onto the anode electrode, there was a uniform thin layer of SLMP on the surface of anode electrode as shown in Fig. 2(b).

Two pouch cells LIC250 and LIC395 were assembled in the dry-room by stacking four double-side coated HC/SLMP anode electrodes, three double-side coated AC cathode electrodes and two single-side coated AC cathode electrodes. The activated carbon material YP-50F was used to assemble the pouch cell LIC250, while LIC395 used cathode material AB-520. Fig. 3 shows the schematic representation and the stacking core of the pouch cells. It can be seen from Fig. 3 that the Cu and Al substrates were welded to nickel (Ni) and aluminum (Al) current collector tabs, respectively. After the stacking and welding processes, the cell core was housed in an aluminum laminated formed case that is suitable for the size of the electrodes. Then the vacuum heat sealing process was applied to the case with the cell core in order to remove the excess gas trapped in the cell after the pouch cells were filled with electrolyte. The separator used was a microporous membrane (Celgard 3501). The electrolyte was 1 M $LiPF_6$ in ethylene carbonate (EC):dimethyl carbonate (DMC) at a ratio of 1:1 by weight (LP30, SelectiLyte™, Merck Electrolyte). Both LIC250 and LIC395 were charged-discharged under various currents in order to obtain the energy density under different discharge C-rate. The LIC pouch cells were then charged and discharged under a charge–discharge C-rate of 20 C to obtain the cycle life performance and the leakage current of the LIC was also tested. The LIC pouch cells were charged and discharged using an Arbin Battery Testing Unit and the electrochemical impedance spectrum (EIS) for LIC250 and LIC395 was recorded in the frequency range of $0.1–10^6$ Hz using Gamry Instruments.

The specific surface area and pore structure of the two kinds of positive electrodes (YP-50F and AB-520) were determined with the nitrogen adsorption/desorption isotherms at 77 K (Quantachrome Autosorb-iQ). All the samples were degassed for 12 h before the adsorption experiments. The specific surface area was calculated by

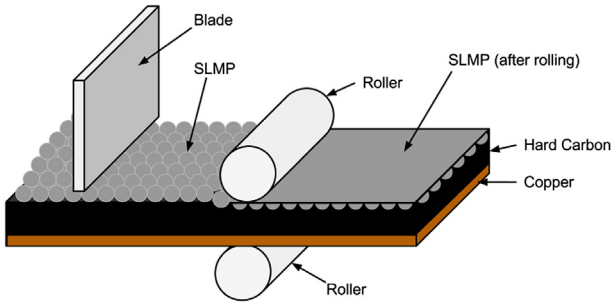

Fig. 1. Schematic view of coating process of stabilized lithium metal powder (SLMP) on the surface of a negative electrode.

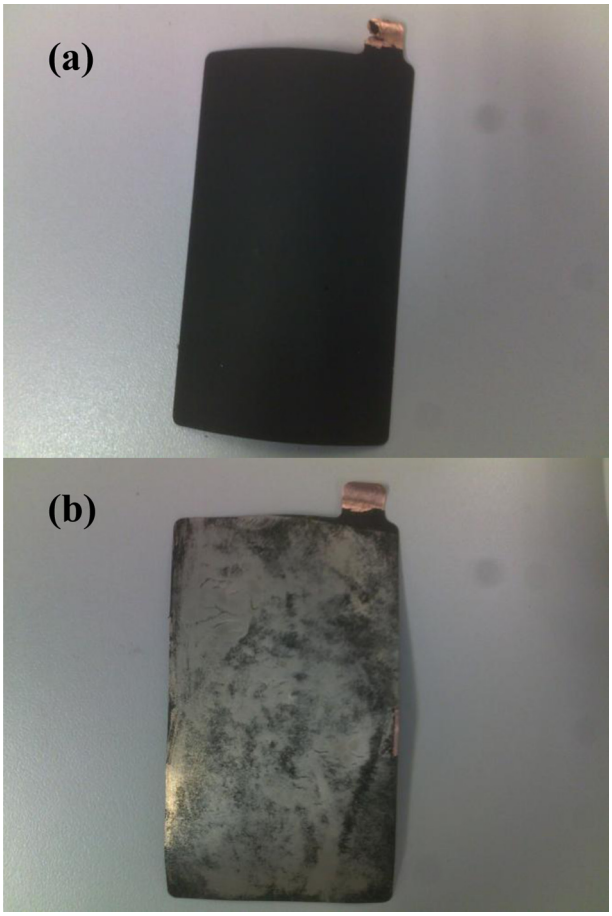

Fig. 2. (a) 8 × 5 cm HC electrode with 1 cm long tab and (b) HC electrode with SLMP pressed on surface.

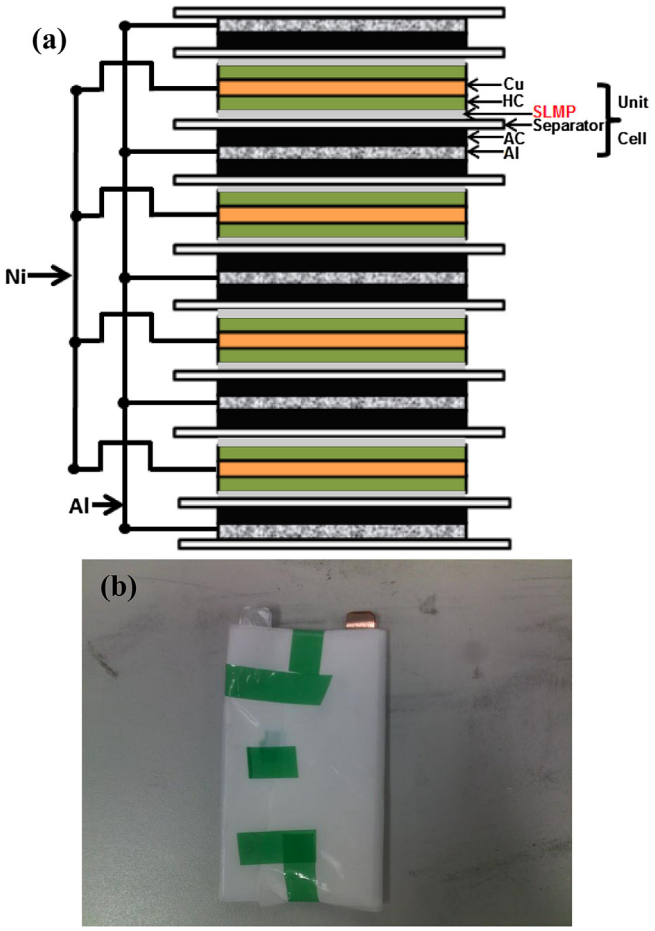

Fig. 3. (a) Schematic representation and (b) stacking core of the LIC pouch cells.

the conventional Brunauer–Emmett–Teller (BET). The total pore volume was estimated by the adsorbed N_2 at a relative pressure of 0.99. The pore size distribution of all the samples was calculated according to the Barett–Joyner–Halenda (BJH) method.

3. Results and discussion

The list of materials used in pouch cells LIC250 and LIC395 are in Table 1. It can be calculated that the density of cathode electrodes YP-50F for LIC250 is about 0.6 g cm^{-3} (Porosity: 70%); while the density of cathode electrodes AB-520 for LIC395 is about 0.74 g cm^{-3} (Porosity: 63%). The density of anode electrodes for both LIC250 and LIC395 is about 1.1 g cm^{-3} (Porosity: 45%). It can be seen from Table 1 that LIC250 contains more electrolyte than LIC395 since the porosity of electrode YP-50F is higher than the electrode AB-520. The LIC250 has a total weight of 20 g and the LIC395 has a total weight of 22 g. Fig. 4 displays the sketch, dimension and picture of the LIC pouch cells.

Table 1
A list of materials used in pouch cells LIC250 and LIC395.

Materials	Weight for LIC250 (g)	Weight for LIC395 (g)	Size (width × length × thickness)
Activated carbon	2.61	3.18	8 cm × 20 cm × 0.03 cm
Hard carbon	2.78	2.78	8 cm × 20 cm × 0.018 cm
SLMP	0.43	0.43	–
Separator	1.02	1.02	8 cm × 50 cm × 0.0025 cm
Electrolyte	6.74	6.0	–
Al foil	0.84	0.84	8 cm × 25 cm × 0.002 cm
Cu foil	1.38	1.38	8 cm × 20 cm × 0.001 cm
PTFE (anode)	0.24	0.24	–
PTFE (cathode)	0.29	0.35	–
Electrode taps Ni (anode)	0.32	0.32	0.8 cm × 4.8 cm × 0.009 cm
Electrode taps Al (cathode)	0.12	0.12	0.8 cm × 4.8 cm × 0.009 cm
Package materials	3.23	5.34	–

Fig. 5 shows the voltage profiles for pouch cells LIC250 and LIC395 for three full cycles in the voltage range of 4.1–2.0 V under a constant current of 100 mA. The energy density and capacitance of LIC250 are 22 Wh kg^{-1} and 250 F; while LIC395 has an energy density of 31.5 Wh kg^{-1} and a capacitance of 395 F, respectively. The calculation of energy density is based on the cell's maximum and minimum voltage of 4.1 and 2.0 V, respectively. Table 2 displays the comparison of energy densities for LIC pouch cells of LIC250 and LIC395. It can be concluded that the energy density of the LIC pouch cell is about 4–6 times more than that of conventional EDLCs, which demonstrates the concept of the high energy density for LIC with this kind of novel electrode composition and cell structure.

To demonstrate the high energy density that LIC can achieve under high-rate charge–discharge, LIC250 and LIC395 were discharged under different current densities. Fig. 6 shows the energy density and power density under different current densities. The current density is calculated by dividing the discharge current by the total weight of the LIC cell. When both the LIC pouch cells were tested under the current 0.1 0.2, 0.4, 1, 2, 4, 6, 8 and 10 A, the energy density of LIC250 is around 22, 21.3, 20.6, 19.7, 18.2, 16, 14.4, 12.4 and 11.2 Wh kg^{-1}, and the energy density of LIC395 is about 31.5, 29.8, 28.6, 26.6, 23.8, 19.6, 16.2, 13.6 and 11.4 Wh kg^{-1}, respectively. It can be obtained from Fig. 6 that LIC250 can deliver an energy

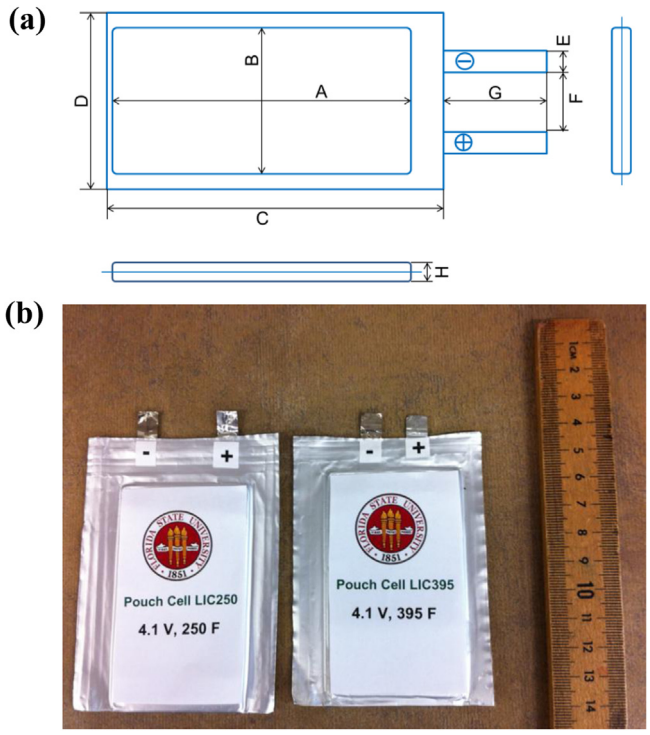

Fig. 4. (a) A sketch of pouch cell and dimension. A (height) = 80 mm, B (width) = 50 mm, C (overall width) = 89 mm, D (overall height) = 55 mm, E (tab width) = 8.0 mm, F (tab distance) = 23 mm, G (tab height) = 0.3 mm, and H (thickness) = 3.6 mm (for LIC250) and 3.9 mm (for LIC395) and (b) Pictures of the high energy density Li-ion capacitor pouch cells.

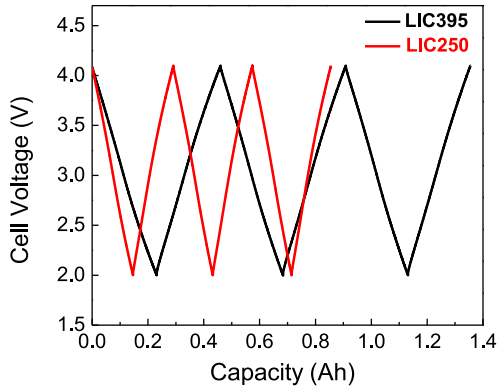

Fig. 5. Galvanostatic charge–discharge profiles of prototypes LIC250 and LIC395 at a constant current of 0.1 A from 2.0 to 4.1 V.

Table 2
Comparison of energy densities for pouch cells LIC250 and LIC395.

Capacitors	LIC250	LIC395
Max. voltage (V)	4.1	4.1
Capacitance (F)	250	395
Weight (g)	20	22
Dimension	5 × 8.9 × 0.36 cm^3	5 × 8.9 × 0.39 cm^3
Specific energy (Wh kg^{-1})	22	31.5
Energy density (Wh L^{-1})	27.5	39.6

density of 11.1 Wh kg^{-1} (50% of the maximum energy) at a discharge C-rate of 123 C and the LIC395 can achieve an energy density of 11.4 Wh kg^{-1} (36.2% of the maximum energy) at a discharge C-rate of 104 C. Although LIC395 has a higher energy density than LIC250, LIC250 can achieve higher power performance than LIC395. The electrochemical impedance spectra (EIS) were performed to both pouch cells as shown in Fig. 7(a). These spectra were recorded in the frequency range from 10 mHz to 1 MHz with a signal amplitude of 10 mV. Both the EIS were fitted by the electric equivalent circuit model [23] as shown in Fig. 7(b) and Table 3 lists fitting parameters for each pouch cell, respectively. It can be seen from Table 3 that the resistance fitting values including the ohmic resistance (R_s) and Warburg element (R_W) of the LIC250 are smaller than that of the LIC395, which explains the different power performance between LIC250 and LIC395. It was found that at high frequencies >100 Hz (the data was not showed in Fig. 6), an inductive behavior was demonstrated due to the stacking structure of the cell as shown in Fig. 3 and measurement cables connected the electrochemical impedance spectrometer to LICs.

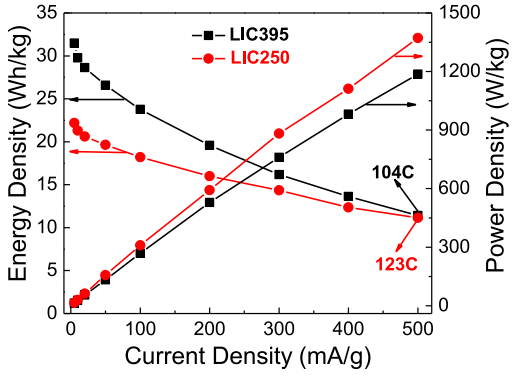

Fig. 6. The energy density and power density as a function of the current densities for pouch cells LIC250 and LIC395.

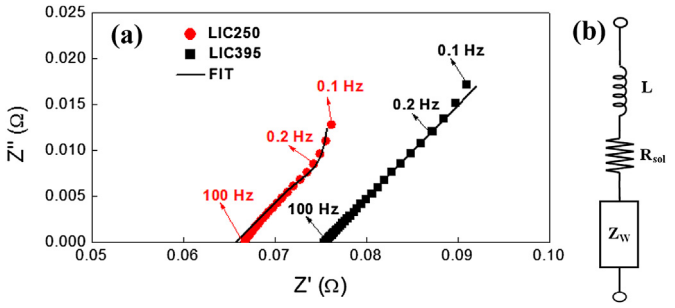

Fig. 7. (a) The EIS of pouch cells LIC250 and LIC395 and (b) the electric equivalent circuit used to fit the EIS.

The only difference between the pouch cell LIC250 and LIC395 is the cathode materials (activated carbon) that were used, so in order to fully understand both LIC250 and LIC395, the nitrogen (N_2) adsorption–desorption isotherms and corresponding pore size distributions for both the activated carbon cathode electrodes YP-50F and AB-520 were studied and compared. It can be seen from Fig. 8(a) that YP-50F and AB-520 both exhibit Type IV isotherm according to the IUPAC classification. In these activated carbons, the uptake of N_2 increased even at high relative pressure (>0.5). In addition, the activated carbons YP-50F shows hysteresis loops on the adsorption/desorption isotherms in the region of 0.5–0.95 of relative pressure, which suggest that considerable amounts of mesopores are present in YP-50F. However, there is no hysteresis for AB520. Pore characteristics were obtained based on the N_2 adsorption–desorption isotherms. The BET specific surface area (BET-SSA) of AB-520 electrode (including the PTFE binder) is about 1394 m^2 g^{-1}, while the BET-SSA of YP-50F electrode is about 1124 m^2 g^{-1}. Compared with YP-50F, AB-520 displays higher BET-SSA, which is the reason that LIC395 can achieve a higher capacitance than LIC250. The different behavior of the cells could be due to the influence of the carbonaceous anode since the capacitance is different, the excursion of the AC could be different and that, in turn, it could affect the anode. The pore size distributions of the commercial activated carbons, determined by the BJH method, are shown in Fig. 8(b). Fig. 8(b) displays the pore volume changes (dV) against the pore diameter. It shows that the AB-520 is an artefact of the BJH on the curve which is more characteristic of a microporous system as shown by the very high specific area obtained by the BET-SSA. The pore size of YP-50F is in the range of about 3–11 nm, which is wider than AB-520. At low charge–discharge rates, the electrolyte ions have time to penetrate into the depth of the pores and additional surface-area is accessed, which explains that the activated carbon (AB-520) with the higher BET specific surface area has higher capacitance at low charge–discharge rate. As the charge–discharge rate increases, electrolyte penetration becomes poorer and less surface area is accessed. Under this condition, larger pores lead to a lower distributed electrolyte resistance and greater electrolyte penetration which can enable the majority of the surface area and hence the capacitance to be utilized more effectively. The wider pore size distributions of YP-50F prove that the activated carbon materials YP-50F can achieve higher power performance

Table 3
Fitting parameters obtained from the pouch cells LIC250 and LIC395.

LIC prototype	R_{sol} (Ω)	Warburg diffusion (Z_W)		
		R_w (Ω)	τ_w (s)	p
LIC250	0.066	0.03	4.8	0.5
LIC395	0.075	0.05	7.0	0.5

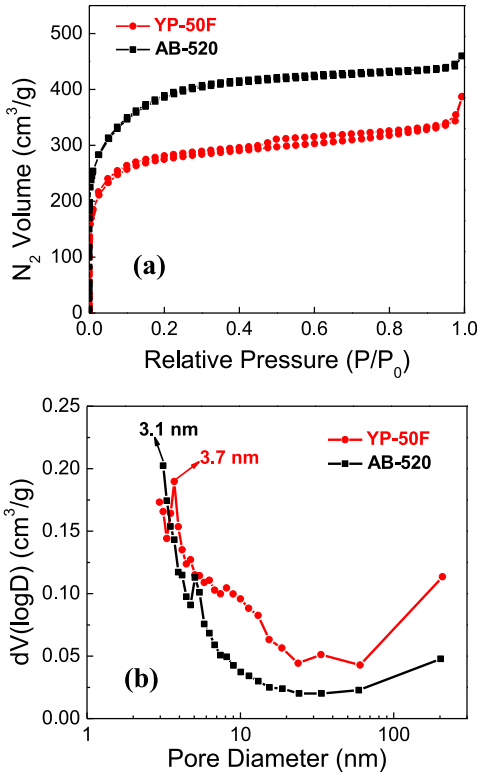

Fig. 8. (a) N_2 adsorption/desorption isotherms and (b) pore size distributions of activated carbons cathode electrodes YP-50F and AB-520.

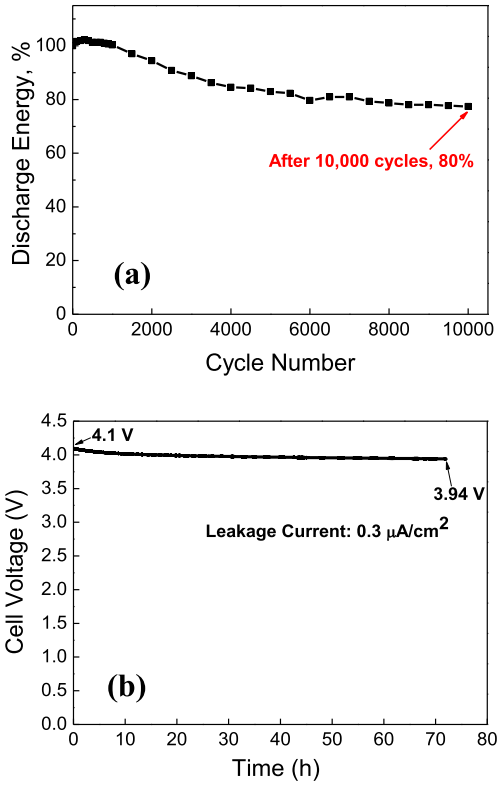

Fig. 9. (a) The specific discharge energy as a function of cycle number for the LIC pouch cells and (b) self-discharge profile of the Li-ion capacitor pouch cell during 72 h.

than AB-520, which illustrates that the LIC250 has better power performance than LIC395. Also, the LIC250 displays larger macroscopic porosity compared to LIC395 since the density of both electrodes is not the same (70% vs. 60%), which best illustrates the difference of the electrochemical performance between LIC250 and LIC395 at high rate. The slight difference at high rate between the two carbons may be indeed related to a lower ionic conductivity in the pores or alternatively to a lower electronic resistivity. From Table 3 and Fig. 7, we can obtain that the high frequency impedance which is higher for AB520/LIC395 may have the two contributions, both ionic and electronic. The higher Warburg for AB520/LIC395 evidences the same contributions at the interface but does not allow discriminating too.

Fig. 9(a) displays the cycling performance for the LIC pouch cells under 4 mA cm^{-2}. It can be seen from Fig. 9(a) that after 5000 cycles, the energy density of the LIC pouch cells became relative stable and the capacitance degradation rate was significant reduced. After 10,000 cycles, the pouch cells still maintained 80% of the initial energy density, which demonstrated the long cycling stability of the LIC pouch cells. Several reports already showed that LIC can be cycled over more than 200,000 without dramatic loss of energy [24], so more work should be done to improve the cycling performance of the SLMP-based 2-electrode structure LIC cells. After the pouch cell was charged to 4.1 V under a constant current, the LIC pouch cell was charged with a 4.1 V constant voltage charge for more than 5 h. Then the cell was rested for 72 h and the cell voltage of the pouch cell was monitored by voltmeter to obtain the self-discharge profile as seen in Fig. 9(b). After an initial IR drop, the voltage decrease as time went on was very little. After 72 h, the cell voltage was stable at 3.94 V. It can be calculated that the leakage current from 0 to 72 h is 0.3 μA cm^{-2} and the leakage current from 36 to 72 h is 0.11 μA cm^{-2}, which indicates that the cell voltage becomes more and more stable as time passes. This leakage current is comparable to the values exhibited in the industrial electric double layer capacitors.

4. Conclusion

Two high energy density Li-ion Capacitor pouch cells, LIC250 with an energy density of 22 Wh kg^{-1} and LIC395 with an energy density of 31.5 Wh kg^{-1} were assembled, studied and compared. LIC250 could maintain 50% of its maximum energy density when it was discharged at a C-rate of 123 C and LIC395 was able to have 36.2% of its maximum energy density when it was discharged at a C-rate of 104 C. The cathode electrodes (YP-50F and AB-520) for both LIC250 and LIC395 were studied and compared by N_2 adsorption–desorption isotherms. Both the LIC pouch cells displayed a cycle life of more than 10,000 cycles and a leakage current as low as 0.3 μA cm^{-2}.

Acknowledgments

This study is supported by DOE BATT Program through PNNL with contract No. 212964 and Florida State University Research Foundation GAPS Program.

References

[1] J.P. Zheng, J. Electrochem. Soc. 150 (2003) A484.
[2] J.P. Zheng, J. Electrochem. Soc. 152 (2005) A1864.
[3] J.P. Zheng, J. Electrochem. Soc. 156 (2009) A500.
[4] G.G. Amatucci, F. Badway, A. DuPasquier, T. Zheng, J. Electrochem. Soc. 148 (2001) A930.
[5] G.G. Amatucci, F. Badway, J. Shelburne, A. Gozdz, I. Plitz, A. DuPasquier, S.G. Menocal, in: Proceedings of the 11th International Seminar on Double Layer Capacitors, Florida Educational Seminars Inc., 2001.
[6] S. Tasaki, N. Ando, M. Nagai, A. Shirakami, N. Matsui, Y. Hato, US Patent Number 7,733,629 B2, June 8, 2010.

[7] H. Konno, T. Kasashima, K. Azumi, J. Power Sources 191 (2009) 623.
[8] M. Schroeder, M. Winter, S. Passerini, A. Balducci, J. Electrochem. Soc. 159 (2012) A1240.
[9] N. Böckenfeld, R. Kühnel, S. Passerini, M. Winter, A. Balducci, J. Power Sources 196 (2011) 4136.
[10] A. Krause, P. Kossyrev, M. Oljaca, S. Passerini, M. Winter, A. Balducci, J. Power Sources 196 (2011) 8836.
[11] T. Aida, I. Murayama, K. Yamada, M. Morita, Electrochem. Solid-State Lett. 10 (2007) A93.
[12] T. Aida, I. Murayama, K. Yamada, M. Morita, J. Electrochem. Soc. 154 (2007) A798.
[13] H. Wang, M. Yoshio, J. Power Sources 195 (2010) 389.
[14] J. Kim, J. Kim, Y. Lim, J. Lee, Y. Kim, J. Power Sources 196 (2011) 10490.
[15] S.R. Sivakkumar, A.S. Milev, A.G. Pandolfo, Electrochim. Acta 56 (2011) 9700.
[16] S.R. Sivakkumar, A.G. Pandolfo, Electrochim. Acta 108 (2012) 280.
[17] A. Brandt, A. Balducci, Electrochim. Acta 65 (2013) 219.
[18] M. Schroeder, M. Winter, S. Passerini, A. Balducci, J. Power Sources 238 (2013) 388.
[19] P.H. Smith, T.N. Tran, T.L. Jiang, J. Chung, J. Power Sources 243 (2013) 982.
[20] J.P. Zheng, W.J. Cao, in: The 20th International Seminar on Double Layer Capacitors and Similar Energy Storage Devices, Florida Educational Seminars Inc., 2010.
[21] W.J. Cao, J.P. Zheng, J. Power Sources 213 (2012) 180.
[22] W.J. Cao, J.P. Zheng, J. Electrochem. Soc. 160 (2013) A1572.
[23] P.L. Moss, J.P. Zheng, G. Au, P.J. Cygan, E.J. Plichta, J. Electrochem. Soc. 154 (2007) A1020.
[24] JSR Micro Catalog, http://www.jsrmicro.com/index.php.